JOURNAL OF CHEMICAL PHYSICS VOLUME 115, NUMBER 3 15 JULY 2001

The lowest doublet and quartet potential energy surfaces involved in the N(^4S)+O$_2$ reaction. I. *Ab initio* study of the C_s-symmetry ($^2A'$, $^4A'$) abstraction and insertion mechanisms

R. Sayós,[a] Carolina Oliva, and Miguel González[a]
Departament de Química Física and Centre de Recerca en Química Teòrica, Universitat de Barcelona, C/Martí i Franquès 1, 08028 Barcelona, Spain

(Received 7 March 2001; accepted 2 May 2001)

In this work we have carried out *ab initio* complete active space self-consistent-field (CASSCF) calculations, second-order perturbation calculations based on CASSCF wave functions (CASPT2), uncontracted multireference configuration interaction calculations, and some density functional calculations with standard correlation-consistent Dunning basis sets and atomic natural orbital basis sets on the lowest $^2A'$ and $^4A'$ potential energy surfaces involved in the title reaction. The ground $^2A'$ surface has an average energy barrier of 5.3 kcal/mol in the CASPT2 complete basis set limit. A peroxy NOO minimum is found in agreement with preceding *ab initio* works, which seems to play an important role in the opening of a double microscopic mechanism: direct C_s abstraction and indirect C_s insertion through the NO$_2$($X\,^2A_1$) molecule. The ground $^4A'$ surface shows an average energy barrier of 13.5 kcal/mol in the CASPT2 complete basis set limit. Despite this excited surface displays another peroxy minimum, in this case only a direct C_s-abstraction mechanism can be expected. The present results improve previous high quality *ab initio* studies and provide lower energy barriers in both potential energy surfaces, which would produce larger total thermal rate constants in better agreement with experimental data. Finally, it is demonstrated that the N and O 2*s* electron correlation cannot be neglected as it produces a significant decrease in both energy barriers.
[DOI: 10.1063/1.1381012]

I. INTRODUCTION

The elementary gas-phase reaction of N(^4S) with molecular oxygen,

$$\mathrm{N}(^4S)+\mathrm{O}_2(X\,^3\Sigma_g^-)\rightarrow \mathrm{O}(^3P)+\mathrm{NO}(X\,^2\Pi),\qquad \Delta_r H^0_{0\,\mathrm{K}}=-32.09\ \mathrm{kcal/mol} \tag{1}$$

(Ref. 1) and its reverse reaction play an important role in atmospheric chemistry. This reaction is a source of infrared chemiluminescence in the upper atmosphere.[2] High temperature studies of the kinetics and dynamics of the N(^4S)+O$_2$ and N(^4S)+NO reactions and their reverse ones are very important for the understanding of the chemical and physical phenomena taking place during the re-entry of spacecrafts into the Earth's atmosphere,[3] where nonthermal equilibrium conditions between the different degrees of freedom may play an essential role. Reaction (1) with hot N atoms provides an additional mechanism for the production of nitric oxide in the earth thermosphere.[4] This reaction is also of interest in the context of combustion of hydrocarbon–air mixtures.[5]

In several preceding papers[6–10] we have presented different theoretical approaches to this reaction and we have also given a detailed review of the main experimental and theoretical data that have been published for this reaction. Thus, in the current introduction we will summarize only the principal information and we will update that with the latest and the most significant contributions to this reaction.

Experimental kinetics studies are available dealing with resembling thermal rate constants in a wide interval of temperatures: $k=1.5\times10^{-11}e^{-3600/T}$ cm^3 molecule^{-1} s^{-1} at 280–910 K (Ref. 11) or $1.5\times10^{-14}T\ e^{-3270/T}$ cm^3 molecule^{-1}s^{-1} at 298–5000 K.[12] Measurements of NO vibrational distributions, populated between $v'=0-7$, show some important differences on their shapes for reactants at room temperature.[13–17]

Several *ab initio* studies have been reported on the ground ($^2A'$) and the first excited ($^4A'$) potential energy surfaces (PES) involved in this reaction. Thus, CASSCF and multireference contracted CI calculations with large Gaussian basis sets[18] have been carried out for both PESs aimed at characterizing the transition states and minimum energy reaction paths. The same *ab initio* method but with large ANO basis sets were also used in a more recent theoretical study of the ground $^2A'$ PES.[19] Several studies have dealt with the controversy about the existence of a NOO peroxy isomer on the ground doublet PES[20–22] that could have some influence in the studied reaction.

In order to study the kinetics and the dynamics of this reaction, several analytical fits of the lowest doublet PES have been reported in previous works based mainly in the before mentioned *ab initio* data.[18,19] Most of them[23,10] are based on the analytical form (many-body expansion) and parameters (diatomic terms and reference structure of the three-body term) employed in our first study,[6] and made use of the

---

[a] Authors to whom correspondence should be addressed. Electronic mail: r.sayos@qf.ub.es and miguel@qf.ub.es

ab initio data of Ref. 18 with some kind of correction in the energy and including experimental diatomic data. Two earlier analytical $^2A'$ PESs, one of bond-order-type based on *ab initio* data,[19] and another of double many-body form based on diatomics-in-molecules (DIM) and *ab initio* data,[24] are available in the literature, although they do not reproduce properly neither the *ab initio* information nor the experimental data. In Ref. 10 we reported a detailed comparison on the transition states for most of these PESs. Regarding to the first excited PES, only one analytical PES is available, which was constructed using a similar procedure than for the ground $^2A'$ PES.[23]

Several quasiclassical trajectory (QCT) studies,[3,6–8,23,25,26] variational transition state theory (VTST) studies[10,19] and quantum approaches[9,27] have been performed to study the kinetics and dynamics of the reaction (1) by using the mentioned PESs.

In the present work we will present a new contribution to the study of the $N(^4S)+O_2$ reaction based on highly accurate and extensive *ab initio* calculations. We initiate a series of papers that will try to study this reaction by using new global analytical PESs ($^2A'$ and $^4A'$) based in the current *ab initio* data. Up to now, the published PESs do not reproduce properly the properties of the $NO_2(X\,^2A_1)$ molecule and its isomers, nor the C_{2v}-insertion mechanism, which involves several surface crossings (i.e., between the $^2A_1$, $^2A_2$, $^2B_1$ and $^2B_2$ PESs). QCT, VTST and wave packet time-dependent quantum dynamics studies will follow the current paper and will try to elucidate the importance of several microscopic mechanisms (i.e., abstraction versus C_s or C_{2v} insertion) that can compete in this reaction as it will be shown in the present work.

Section II will offer a summary of the *ab initio* and density functional theory (DFT) procedures used in this work. Section III will provide the *ab initio* and DFT results on the stationary points of both PESs ($^2A'$ and $^4A'$), and the corresponding minimum energy reaction paths (MERP) connecting minima (MIN) and transition states (TS). Finally, Sec. IV will summarize the concluding remarks.

II. THEORETICAL METHODS

The *ab initio* calculations presented in this work have been performed with the MOLCAS 4.1 (Ref. 28) package of programs. The complete active space self-consistent-field method (CASSCF)[29,30] was employed throughout this study, always choosing the lowest root in C_s symmetry for both the doublet and the quartet PESs (i.e., $^2A'$ and $^4A'$), which correlate reactants and products of reaction (1). The location of each stationary point geometry on the PESs was achieved by optimization searches of both minima and transition states employing analytic CASSCF gradients. Full characterization of them was effected by calculating the numerical Hessian matrix at the optimized geometries. Calculations at second-order perturbation theory based on a zeroth-order CASSCF wave function (CASPT2 method) using the standard correction (i.e., std) or some $G_i(i=1,2,3)$ variants[31] as implemented in MOLCAS 4.1 were applied to refine the stationary points obtained at the CASSCF level. In some cases a grid of CASPT2 points was generated to search directly the stationary point. Thus, local fits were performed by means of bicubic splines[32] or Taylor expansions in the bond angle together with symmetry adapted internal coordinates expansion in the bond lengths to obtain the optimal geometry and the harmonic frequencies at CASPT2 level by using the SURVIBTM code of molecular rovibrational analysis.[33] More details of the procedure used can be found in a recent paper of our group.[34]

Two different active spaces of the NO_2 system were used in the present study: (a) the full-valence active space, i.e., all the atomic $2s$ and $2p$ electrons are distributed among the corresponding derived bonding and antibonding molecular orbitals (MO) [i.e., CAS (17,12)] and (b) a smaller active space with only the $2p$ electrons [i.e., CAS (11,9)]. This latter active space has been assumed to be accurate enough for this system in some preceding papers;[18,19,22] in both cases the natural MO occupation has been checked for all stationary points. The CAS (17,12) comprising 17 electrons in 12 orbitals generates 28 503 and 20 376 configuration state functions (CSF) for the $^2A'$ and $^4A'$ PESs, respectively, while the CAS (11,9) produces only 3048 and 1878, respectively.

CASPT2 and CASSCF calculations have been performed checking the effect of the correlation energy of the three atomic $1s$ or $2s$ electrons; previously, the $1s$ and $2s$ orbitals were optimized at the CASSCF level. The results were very similar to those obtained previously without the $1s$ frozen core option. In all cases the barrier energies were around 10% higher if the $1s$ orbitals were kept frozen. $2s$ valence orbitals were only kept frozen in some CASPT2 calculations to compare with earlier CASSCF followed by multireference contracted CI (CCI) calculations.[18]

The standard correlation-consistent (cc-pVnZ and aug-cc-pVnZ, $n=$D,T,Q,5) Dunning's basis sets[35] and small and large atomic natural orbital (ANO) basis sets[36] were used in the present study. The basis sets were obtained from the Extensible Computational Chemistry Environment Basis Set Database, version 1.0, as developed and distributed by the Molecular Science Computing Facility.[37]

Some density functional theory (DFT) studies by using the unrestricted B3LYP method as implemented in the GAUSSIAN 98 (Ref. 38) code were adopted to facilitate the search of the stationary points.

Supermolecule calculations were considered in the determination of all energies in both the *ab initio* and the DFT methods.

Recent studies on similar reactions [e.g., $N(^2D)+NO$ (Ref. 34) and $N(^2D)+O_2$,[39] systems] using the present methods have shown that they are accurate enough to provide a good description of them in comparison with experimental data or larger calculations.

III. RESULTS AND DISCUSSION

A. Stable molecules and reaction exoergicity

A first verification of the degree of accuracy of the theoretical approach has been carried out by calculating the properties of the diatomic and $NO_2(X\,^2A_1)$ molecules, and the exoergicity of reaction (1). Thus, Table I summarizes the

TABLE I. *Ab initio* and DFT properties of reactants and products.[a]

Method	Basis set[b]	N(^4S)+O$_2$				O(^3P)+NO				ΔD_e[c]
		E/a.u.	R_e/Å	ω_e/cm^{-1}	D_e/kcal mol^{-1}	E/a.u.	R_e/Å	ω_e/cm^{-1}	D_e/kcal mol^{-1}	kcal mol^{-1}
CASSCF(11,9)	ANO-A	−204.163 165	1.2158	1544.05	87.12	−204.220 540	1.1564	1904.66	123.12	−36.00
	ANO-D	−204.166 589	1.2140	1554.00	88.76	−204.224 162	1.1548	1905.66	124.89	−36.13
	cc-pVDZ	−204.097 256	1.2188	1539.25	83.96	−204.153 884	1.1620	1926.57	119.50	−35.53
	cc-pVTZ	−204.149 390	1.2160	1545.95	88.32	−204.206 461	1.1565	1908.11	124.13	−35.81
	cc-pVQZ	−204.163 535	1.2140	1554.42	88.90	−204.221 166	1.1547	1908.18	125.05	−36.16
	aug-cc-pVDZ	−204.109 068	1.2188	1552.25	86.15	−204.165 425	1.1636	1907.45	121.50	−35.36
	aug-cc-pVTZ	−204.151 544	1.2161	1545.00	88.44	−204.208 744	1.1564	1899.72	124.32	−35.89
CASPT2(11,9) std	cc-pVDZ	−204.453 842			109.17	−204.488 174			130.70	−21.54
	cc-pVTZ	−204.661 455			119.68	−204.697 356			142.21	−22.53
	cc-pVQZ	−204.770 974			121.99	−204.807 859			145.12	−23.15
	aug-cc-pVDZ	−204.496 305			112.05	−204.528 300			132.13	−20.08
	aug-cc-pVTZ	−204.679 268			122.26	−204.715 208			144.82	−22.55
CASPT2(11,9) G1	cc-pVTZ	−204.650 644			122.84	−204.692 400			149.04	−26.20
CASPT2(11,9) G2	cc-pVDZ	−204.444 018			111.86	−204.484 042			136.98	−25.12
	cc-pVTZ	−204.649 435			122.93	−204.690 010			148.39	−25.46
	cc-pVQZ	−204.758 182			125.54	−204.799 998			151.78	−26.24
	aug-cc-pVDZ	−204.485 080			115.42	−204.521 330			138.15	−22.75
	aug-cc-pVTZ	−204.666 579			125.84	−204.707 424			151.46	−25.63
CASPT2(11,9) G3	cc-pVTZ	−204.650 092			123.35	−204.690 174			148.48	−25.15
CASSCF(17,12)	ANO-A	−204.168 563	1.2176	1539.78	90.51	−204.229 351	1.1586	1892.17	128.65	−38.14
	ANO-B	−204.171 284	1.2164	1547.15	91.80	−204.232 117	1.1576	1891.29	129.97	−38.17
	ANO-C	−204.171 804	1.2158	1549.40	92.06	−204.776 429	1.1572	1892.88	130.31	−38.26
	cc-pVDZ	−204.102 678	1.2206	1534.14	87.37	−204.162 890	1.1640	1914.40	125.15	−37.78
	cc-pVTZ	−204.154 781	1.2178	1541.57	91.71	−204.215 300	1.1588	1895.30	129.67	−37.97
	cc-pVQZ	−204.168 923	1.2157	1550.09	92.29	−204.229 002	1.1570	1895.67	130.61	−37.70
	aug-cc-pVDZ	−204.114 455	1.2205	1547.48	89.52	−204.174 351	1.1657	1894.98	127.11	−37.59
	aug-cc-pVTZ	−204.156 929	1.2179	1540.81	91.80	−204.217 565	1.1586	1888.68	129.83	−38.05
CASPT2(17,12) std	cc-pVDZ	−204.454 466			109.56	−204.490 850			132.39	−22.83
	cc-pVTZ	−204.661 638			119.80	−204.696 977			141.96	−22.18
	cc-pVQZ	−204.771 209			122.13	−204.810 032			146.48	−24.36
	aug-cc-pVDZ	−204.496 814			112.37	−204.530 891			133.77	−21.38
	aug-cc-pVTZ	−204.679 556			122.45	−204.717 462			146.22	−23.79
CASPT2(17,12) G2	ANO-A	−204.628 665			123.23	−204.669 150			148.64	−25.40
	ANO-B	−204.700 404			126.60	−204.744 705			154.41	−27.80
	ANO-C	−204.732 620			128.38	−204.776 429			155.86	−27.49
	cc-pVDZ	−204.444 535			112.19	−204.484 605			137.35	−25.14
	cc-pVTZ	−204.649 724			123.12	−204.691 974			149.61	−26.51
	cc-pVQZ	−204.758 313			125.63	−204.802 022			153.05	−27.43
	aug-cc-pVDZ	−204.485 486			115.67	−204.523 776			139.70	−24.03
	aug-cc-pVTZ	−204.666 762			125.93	−204.709 530			152.77	−26.84
CASPT2(17,12) G3	cc-pVTZ	−204.650 378			123.51	−204.692 886			150.19	−26.67
CASPT2(17,12) G2[d]	aug-cc-pVTZ	−204.666 873	1.2087	1583.13	125.95	−204.709 581	1.1532	1899.21	153.16	−26.80
UB3LYP	aug-cc-pVTZ	−204.987 508	1.2055	1626.28	123.16	−205.037 417	1.1455	1967.77	154.48	−31.32
Experimental[e]			1.2075	1580.19	120.22		1.1508	1904.20	152.53	−32.31

[a] CASPT2 energies at the CASSCF optimum geometries with the same basis set.

[b] ANO basis sets are $A[14s9p4d3f/4s3p2d1f]$, $B[14s9p4d3f/6s4p3d2f]$, $C[14s9p4d3f/6s5p4d3f]$, $D[14s9p4d3f/7s6p4d3f]$ (Ref. 36).

[c] Reaction exoergicity for N(^4S)+O$_2$→O(^3P)+NO.

[d] CASPT2 G2 optimum geometries and harmonic vibrational frequencies obtained by using the VIBROT module of the MOLCAS 4.1 program (Ref. 28). Masses of the most abundant isotopes were used: ^{14}N and ^{16}O.

[e] The lowest spin–orbit states [i.e., NO($X\,^2\Pi_{1/2}$) and O($^3P_2$)] were used for the experimental data (Ref. 40).

bond length, the harmonic vibrational frequency and the dissociation energy of both diatomic molecules at different *ab initio* levels. The comparison of the calculated geometries with the experimental data shows a small effect of the size and quality of the basis set on the optimized bond length, although the most remarkable enhancement is produced when the geometry is optimized directly at the CASPT2 G2 level. The results are comparable for both types of basis sets (i.e., ANO and cc-pVnZ/aug-cc-pVnZ) for a similar number of basis functions (e.g., compare the ANO-A basis set with the cc-pVTZ one both with a total number of 90 basis functions). An excellent agreement was also obtained for the harmonic frequencies. However, the description of both O$_2$ and NO dissociation energies was somewhat worse. First, the introduction of the dynamical correlation energy by means of the CASPT2 method was essential for a reasonable description. Second, the G_i variants gave similar results although much better than the standard Fock matrix one, as it should be expected.[31] The O$_2$ dissociation energy presented a significant error (4.5% with respect to the experimental value) even at the highest *ab initio* calculation level [i.e., CASPT2 G2(17,12)/aug-cc-pVTZ method], that originated mainly the discrepancy in the exoergicity with respect to the experimental value. The differences arised from the use of two different active spaces were very small as should be expected owing to the high occupation number [over 1.99 in CAS(17,12)] of two of the natural MOs in this asymptotic region of the PES.

The difficulty in the O_2 theoretical treatment is well known and can only be amended with very refined and computationally expensive *ab initio* calculations with inclusion of complete basis set (CBS) limits.[41,42] However, we believe that is not crucial in the context of the present study, which tries to account for all the stationary points of the lowest doublet and quartet PESs at the same level, with a foremost importance concerning the energy barriers.

On the other hand, DFT calculations at the UB3LYP/aug-cc-pVTZ level offered good results and improved substantially the reaction exoergicity.

Table II presents the results for the $NO_2(X\,^2A_1)$ molecule. In spite of the calculated geometry and harmonic frequencies were very similar for both actives spaces [i.e., (11,9) and (17,12)] and match very well the experimental values, important differences were observed in the dissociation energies. The increase of the active space size improved significantly the calculated dissociation energies, although was necessary the introduction of the dynamical correlation energy by means of the CASPT2 method to accurately reproduce the experimental values. The reference weight into the CASPT2 wave function was high enough to describe properly the molecule [i.e., approximately 90% at CAS(17,12)]. The importance of the higher active space was confirmed by the occupation of the 12 natural MOs: a_1:1.998, 1.984, 1.980, 1.039, 0.0424, b_1:1.965, 0.115, a_2:1.923, and b_2:1.998, 1.966, 1.960, 0.0284. The nitrogen $2s$ contribution in several active MOs was important in the description of the NO_2 molecule, especially for bent geometries as it has been also observed in previous works.[49] On the other hand, the multireference character of the wave function of the NO_2 molecule can be clearly illustrated taking into account the three most important CSFs and their coefficients:

$$\begin{array}{ll}
-0.943 & \cdots(3a_1)^2(4a_1)^2(5a_1)^2(6a_1)^1(7a_1)^0(1b_1)^2(2b_1)^0(1a_2)^2(2b_2)^2(3b_2)^2(4b_2)^2(5b_2)^0,\\
-0.144 & \cdots(3a_1)^2(4a_1)^2(5a_1)^2(6a_1)^2(7a_1)^0(1b_1)^2(2b_1)^0(1a_2)^2(2b_2)^2(3b_2)^2(4b_2)^1(5b_2)^0,\\
0.125 & \cdots(3a_1)^2(4a_1)^2(5a_1)^2(6a_1)^1(7a_1)^0(1b_1)^2(2b_1)^2(1a_2)^0(2b_2)^2(3b_2)^2(4b_2)^2(5b_2)^0.
\end{array} \tag{2}$$

The present study improves the previous *ab initio* results for NO_2 molecule as it can be observed in Table II.

B. Characterization of the lowest $^2A'$ potential energy surface

The geometries, frequencies, and energies relative to reactants, $N(^4S)+O_2$, for all the stationary points characterized at the *ab initio* (i.e., CASSCF and CASPT2) and DFT (i.e., UB3LYP) levels for the ground doublet PES are given in Tables III, IV, and V. Figure 1 shows the MERPs connecting reactants and products. The attack of the $N(^4S)$ atom to the O_2 molecule produces a bent transition state (TS1) with the highest energy barrier along the MERP, which leads to a shallow NOO peroxy minimum (MIN1) previously reported in the literature.[21,22]

The system can directly produce $O(^3P)+NO$ after surmounting another transition state (TS2) or can evolve through another shallow NOO minimum (MIN2) and through the much deeper ground state $NO_2(X\,^2A_1)$ molecule after surmounting two transition states (TS3 and TS4). No barrier seems to exist between NO_2 molecule and products. Table III presents a comparative study about the properties of TS1. First of all, CASSCF calculations with different basis sets and the lower active space (11,9) yield similar geometries, frequencies and a very small decrease in the energy barrier. Nevertheless, the increase in the active space to (17,12) produces a significant enlargement of the NO distance (ca., 0.025 Å) and also an additional energy barrier reduction. The introduction of the dynamical correlation energy through the CASPT2 method (std or G2) originates a dramatic decrease in the energy barrier. In some cases the obtained value [e.g., 4.14 kcal/mol at CASPT2(17,12) G2/aug-cc-pVTZ] is too small in comparison with a value compatible with the experimental activation energy [i.e., 7.2 kcal/mol within 280–910 K (Ref. 11)]. Due to this fact, and also taking into account previous published results (see Table III) that evidence the important effect of the dynamical correlation energy into the NO distance optimization of this TS [e.g., 1.821 Å at MR–CCI+Q/CASSCF(11,9)/[$11s6p$/$5s3p2d1f$]][18] or 1.825 Å at MR–ICCI+Q/CASSCF(9,8)/cc-pVTZ[22]], we carried out a numerical optimization at the CASPT2(17,12) G2 level. An optimum NO distance of 1.825 Å was obtained for TS1, which produced an energy barrier of 4.70 kcal/mol [5.00 kcal/mol including zero point energy (ZPE) differences].

A detailed study of the energy barrier of TS1 has been made by increasing the quality of the basis set at the optimum CASPT2(17,12) G2 geometry. The basis set dependence is usually well described by a simple exponential-like function[50] of the form

$$\Delta E_n^{\neq} = \Delta E_\infty^{\neq} + Be^{-Cn}, \tag{3}$$

where n is the cardinal number of the basis set (2, 3, 4, and 5 for DZ, TZ, QZ, and 5Z, respectively) and $\Delta E_\infty^{\neq}$ corresponds to the estimated complete basis set (CBS) limit as $n\rightarrow\infty$. The estimated CASPT2(17,12) CBS limits for this

TABLE II. *Ab initio* and DFT properties of the $NO_2(X\ ^2A_1)$ molecule.[a]

Method	Basis set[b]	E/a.u.	$R_{e(\mathrm{NO})}$/Å	<ONO/°	ω_i/cm^{-1} [c]			D_e/kcal mol^{-1} [d]	
CASSCF(11,9)	ANO-A	−204.279 148	1.1969	134.28	1336.73	758.36	1643.68	36.78	72.78
	ANO-D	−204.283 923	1.1959	134.23	1338.00	761.73	1642.64	37.50	73.63
	cc-pVDZ	−204.207 210	1.2026	133.95	1342.90	752.37	1654.58	33.46	69.00
	cc-pVTZ	−204.265 605	1.1977	134.21	1335.73	758.95	1645.62	37.10	72.92
	cc-pVQZ	−204.281 099	1.1959	134.22	1340.21	762.90	1645.30	37.61	73.77
	aug-cc-pVDZ	−204.221 811	1.2037	133.93	1335.32	747.23	1641.91	35.37	70.75
	aug-cc-pVTZ	−204.268 151	1.1973	134.23	1331.92	759.00	1637.15	37.29	73.17
CASPT2(11,9) std	cc-pVDZ	−204.595 240						67.17	88.73
	cc-pVTZ	−204.819 314						76.54	99.07
	cc-pVQZ	−204.932 603						78.29	101.42
	aug-cc-pVDZ	−204.641 007						70.73	90.81
	aug-cc-pVTZ	−204.841 480						79.23	101.79
CASPT2(11,9) G2	cc-pVDZ	−204.597 127						70.96	96.07
	cc-pVTZ	−204.800 811						69.53	94.98
	cc-pVQZ	−204.934 093						84.15	110.39
	aug-cc-pVDZ	−204.642 824						76.24	99.00
	aug-cc-pVTZ	−204.843 002						85.07	96.00
CASSCF(17,12)	ANO-A	−204.306 726	1.2035	134.01	1339.95	751.77	1614.86	48.56	86.71
	ANO-B	−204.310 264	1.2028	133.95	1340.85	754.60	1614.98	49.05	87.21
	cc-pVDZ	−204.235 397	1.2087	133.80	1348.46	746.83	1632.93	45.50	72.92
	cc-pVTZ	−204.293 276	1.2043	133.95	1339.62	752.71	1618.38	48.93	86.91
	cc-pVQZ	−204.308 694	1.2025	133.94	1343.13	755.82	1616.13	50.02	87.70
	aug-cc-pVDZ	−204.249 666	1.2100	133.78	1341.69	742.21	1618.21	47.25	84.84
	aug-cc-pVTZ	−204.295 723	1.2040	133.95	1335.76	753.15	1608.79	49.05	87.10
CASPT2(17,12) std	cc-pVDZ	−204.594 659						65.14	87.97
	cc-pVTZ	−204.817 849						75.84	98.03
	cc-pVQZ	−204.930 986						75.89	108.36
	aug-cc-pVDZ	−204.640 114						68.53	89.91
	aug-cc-pVTZ	−204.839 859						76.81	100.59
CASPT2(17,12) G2	ANO-A	−204.795 983						79.58	104.99
	ANO-B	−204.875 660						82.16	109.97
	cc-pVDZ	−204.593 065						68.05	93.21
	cc-pVTZ	−204.816 027						77.85	104.35
	cc-pVQZ	−204.929 061						79.72	107.14
	aug-cc-pVDZ	−204.638 534						72.02	96.04
	aug-cc-pVTZ	−204.837 976						80.59	107.44
CASPT2(17,12) G2[e]	aug-cc-pVTZ	−204.838 117	1.1965	134.30	1344.13	755.27	1677.17	80.69	107.52
OVC–CI[f]	Dunning $[9s5p/4s3p1d]$		1.199	134.5	1351	758			
CISD[g]	QZ+2P	−204.652 64	1.174	135.1	1502	809	1821		
CASPT2(11,9)[h]	Dunning DZ+P		1.23	137.5	1568	694	1473	69.49	
UB3LYP	aug-cc-pVTZ	−205.160 469	1.1912	134.45	1385.88	766.12	1688.07	77.22	108.53
Experiment[i]			1.19455	133.851					
[j]								74.48	106.79[m]
[k]			1.197	134.25	1357.8	756.8	1665.5		
[l]			1.1937	134.1	1319.7	749.8	1617.75	71.83	103.90

[a] CASPT2 energies at the CASSCF optimum geometries with the same basis set.

[b] ANO basis set as in Table I.

[c] Harmonic vibrational frequencies: ω_s (sym str, a_1), ω_b (bend, a_1), and ω_a (asym str, b_2), respectively (YZ taken as the molecular plane). Masses of the most abundant isotopes were used: ^{14}N and ^{16}O.

[d] Dissociation energies to the $O(^3P)+NO$ and $N(^4S)+O_2$ asymptotes, respectively.

[e] CASPT2 G2 optimum geometries and harmonic vibrational frequencies obtained by using the SURVIBTM program (Ref. 33).

[f] Reference 43.

[g] Reference 44.

[h] Reference 45. Properties derived from an analytical fit of 872 *ab initio* points.

[i] Reference 46.

[j] Reference 47.

[k] Reference 1. Fundamental v_i frequencies are reported.

[l] Reference 48. Fundamental v_i frequencies are reported.

[m] Obtained by adding the experimental exoergicity (Ref. 40).

energy barrier were (a) 4.90 and 4.73 kcal/mol at the G2 level, and (b) 5.99 and 5.69 kcal/mol at the std level for the cc-pVnZ and aug-cc-pVnZ series, respectively, with a maximum error of ± 0.3 kcal/mol, estimated by using other exponential functions. Therefore, similar CBS energy barriers were found for both series of basis sets. The main difference (ca., 1 kcal/mol) arises from the use of the G2 or the standard CASPT2 variants. However, these values are very close to

TABLE III. *Ab initio* and DFT properties for the entrance channel transition state (TS1) on the $^2A'PES$.[a]

Method	Basis set[b]	E/a.u.	$R_{e(\mathrm{NO})}$/Å	$R_{e(\mathrm{OO})}$/Å	<NOO/°	ω_i/cm^{-1} [c]			ΔE/kcal mol^{-1} [d]
CASSCF(11,9)	ANO-A	−204.132 389	1.7343	1.2406	113.43	653.20i	413.03	1307.05	19.31(19.56)
	cc-pVDZ	−204.064 275	1.7040	1.2499	112.79	673.23i	424.96	1258.55	20.69(20.90)
	cc-pVTZ	−204.118 473	1.7332	1.2415	113.24	657.19i	413.96	1304.88	19.40(19.65)
	cc-pVQZ	−204.132 851	1.7357	1.2384	113.38	654.79i	413.67	1317.82	19.25(19.50)
	aug-cc-pVDZ	−204.078 236	1.7310	1.2442	112.74	650.45i	413.76	1308.07	19.35(19.59)
	aug-cc-pVTZ	−204.121 279	1.7392	1.2404	113.32	647.97i	413.61	1311.54	18.99(19.25)
CASPT2(11,9) std	cc-pVDZ	−204.433 397							12.83
	cc-pVTZ	−204.647 335							8.86
	cc-pVQZ	−204.758 841							7.61
	aug-cc-pVDZ	−204.481 532							9.27
	aug-cc-pVTZ	−204.669 655							6.03
CASPT2(11,9) G2	cc-pVDZ	−204.428 068							10.1
	cc-pVTZ	−204.640 027							5.90
	cc-pVQZ	−204.750 764							4.65
	aug-cc-pVDZ	−204.474 120							6.88
	aug-cc-pVTZ	−204.660 679							3.70
CASSCF(17,12)	ANO-A	−204.141 680	1.7581	1.2404	113.98	636.43i	392.01	1316.25	16.87(17.11)
	cc-pVDZ	−204.073 933	1.7287	1.2493	113.33	658.28i	402.20	1269.32	18.04(18.24)
	cc-pVTZ	−204.127 685	1.7578	1.2413	113.73	640.20i	392.44	1314.40	17.00(17.24)
	cc-pVQZ	−204.142 118	1.7605	1.2881	113.89	636.23i	392.93	1327.83	16.82(17.06)
	aug-cc-pVDZ	−204.087 573	1.7563	1.2438	113.26	633.22i	391.36	1314.98	16.87(17.10)
	aug-cc-pVTZ	−204.130 511	1.7649	1.2402	113.76	633.32i	384.91	1318.26	16.58(16.81)
CASPT2(17,12) std	cc-pVDZ	−204.434 858							12.30
	cc-pVTZ	−204.648 144							8.47
	cc-pVQZ	−204.759 537							7.32
	aug-cc-pVDZ	−204.483 024							8.65
	aug-cc-pVTZ	−204.670 927							5.41
CASPT2(17,12) G2	ANO-A	−204.622 655							3.77
	cc-pVDZ	−204.428 408							10.12
	cc-pVTZ	−204.639 402							6.48
	cc-pVQZ	−204.750 175							5.11
	aug-cc-pVDZ	−204.474 234							7.06
	aug-cc-pVTZ	−204.660 158							4.14
CASPT2(17,12) G2[e]	aug-cc-pVTZ	−204.659 275	1.8565	1.2207	115.88	414.72i	354.08	1438.94	4.70(5.00)
UB3LYP	aug-cc-pVTZ	−204.978 257	1.8647	1.2207	114.21	454.68i	347.08	1439.11	5.81(6.03)
CASSCF(11,9)[f]	Duijneveldt $[11s6p/5s3p2d1f]$		1.730	1.253	114.1	702i	367	1294	18.4(18.5)
MR–CCI+Q/CASSCF(11,9)[f]	Duijneveldt $[11s6p/5s3p2d1f]$		1.821	1.233	115.0	505i	370	1498	10.2(10.6)
CASSCF(11,9)[g]	ANO-A		1.736	1.240	113.5				19.3
MR–CI+Q/CASSCF(11,9)[g]	ANO-A		1.818	1.225	114.0				8.8
MR–ICCI+Q/CASSCF(9,8)[h]	cc-pVTZ	−204.376 00	1.825	1.232	113.8	626i	398	1252	11.72[i]

[a] CASPT2 energies at the CASSCF optimum geometries with the same basis set.

[b] ANO-A basis set: $[14s9p4d3f/4s3p2d1f]$ (Ref. 36).

[c] Harmonic vibrational frequencies: ω_1 (NO str, a'), ω_2 (NOO bend, a'), and ω_3 (OO str, a'), respectively. Masses of the most abundant isotopes were used: ^{14}N and ^{16}O.

[d] Energy barrier respect to N(^4S)+O$_2$. The value corrected with the difference of zero point energies is shown in parentheses.

[e] CASPT2 G2 optimum geometries and harmonic vibrational frequencies obtained by using the SURVIBTM program (Ref. 33).

[f] Reference 18.

[g] Reference 19.

[h] Reference 22.

[i] A value of 8.6 kcal mol^{-1} was extrapolated assuming the effects of basis set and correlation of the O($2s$) and N($2s$) were additive (Ref. 22).

the energy barrier finally fitted in our previous analytical PES (i.e., 6.2 kcal/mol[10]), which was derived from *ab initio* data[18] and variational transition state rate constants which reproduced the experimental rate constants in a wide interval of temperatures (300–5000 K), with the inclusion of the $k(^4A')$ contribution.

We have also calculated the TS1 energy barrier using the uncontracted multireference SD–CI (MR–CI) method with the inclusion of the Davidson correction (Q), based on the same CASSCF(11,9) MOs; 11 e have been correlated ($1s$ and $2s$ electrons were frozen). We have done these calculations to verify the previous results of Walch and Jaffe[18] (Table III) and to show how those MR–CI+Q calculations overestimate energy barriers, specially when the $2s$ electrons are not correlated. We have obtained an energy barrier of 8.16 kcal/mol by using a MR–CI with 24 CSFs of reference (3.709.673 CSF in all for C_s symmetry). If the $2s$ electrons are neither correlated in the CASPT2(11,9) G2 calculations, the barrier increases to 8.07 kcal/mol, which is very similar to the mentioned MR–CI+Q value. Therefore, it is very important to correlate the $2s$ electrons in both the CASPT2 and MR–CI calculations, which produces lower energy barriers,

TABLE IV. *Ab initio* and DFT properties of the NOO($^2A'$) peroxy minimum (MIN1).[a]

Method	Basis set	E/a.u.	$R_{e(\mathrm{NO})}$/Å	$R_{e(\mathrm{OO})}$/Å	<NOO/°	ω_i/cm^{-1} [b]			ΔE/kcal mol^{-1} [c]	
CASSCF(17,12)	cc-pVDZ	−204.103 826	1.2333	1.3802	119.98	1158.55	284.77	608.61	37.06	−0.72
	cc-pVTZ	−204.163 220	1.2255	1.3674	120.62	1168.29	323.31	686.75	32.68	−5.30
	cc-pVQZ	−204.178 556	1.2221	1.3651	120.73	1177.26	334.49	680.70	31.66	−9.43
	aug-cc-pVDZ	−204.120 972	1.2349	1.3723	118.11	1171.40	352.77	624.31	33.50	−4.09
	aug-cc-pVTZ	−204.166 630	1.2232	1.3700	120.35	1176.86	335.96	660.22	31.96	−6.09
CASPT2(17,12) G2	cc-pVDZ	−204.456 657							17.54	−7.61
	cc-pVTZ	−204.677 815							8.88	−17.63
	cc-pVQZ	−204.790 834							7.02	−20.41
	aug-cc-pVDZ	−204.505 818							11.27	−12.76
	aug-cc-pVTZ	−204.700 644							5.58	−21.26
CASPT2(17,12) G2[d]	aug-cc-pVTZ	−204.701 014	1.2170	1.3491	123.81	1320.48	252.17	857.50	5.34	−21.49
UB3LYP	aug-cc-pVTZ	−205.025 026	1.1952	1.3577	124.74	1231.40	373.99	772.71	7.78	−23.54
MR–ICCI+Q/CASSCF(9,8)[e]	cc-pVTZ	−204.399 24	1.257	1.328	114.9	1238	509	979	17.73[g]	−14.58
CASSCF(17,12)[f]	DZ+P	−204.138 98	1.255	1.365	118.6	1116	356	761		
CISD[f]	QZ+2P	−204.513 50	1.160	1.371	121.2	1639	506	519		

[a] CASPT2 energies at CASSCF geometries.

[b] Harmonic vibrational frequencies: ω_1 (NO str, a'), ω_2 (NOO bend, a'), and ω_3 (OO str, a'), respectively. Masses of the most abundant isotopes were used: ^{14}N and ^{16}O.

[c] Energy respect to O(^3P)+NO and N(^4S)+O_2, respectively. In Ref. 21 relative energies to NO_2($X\,^2A_1$) were given, here ΔE has been obtained by using the NO_2($X\,^2A_1$) experimental dissociation energies (Ref. 46).

[d] CASPT2(17,12) energies, geometries, and harmonic vibrational frequencies derived from a grid of points by using the SURVIBTM program (Ref. 33).

[e] Reference 22.

[f] Reference 21. The energy referred to NO_2($X\,^2A_1$) was 75.3 and 85.3 kcal mol^{-1} at CASSCF(17,12)/DZ+P and CISD+Q/QZ+2P levels, respectively. We obtained 81.01, 86.14, and 84.99 kcal mol^{-1} at CASSCF(17,12)/aug-cc-pVTZ, CASPT2(17,12) G2/aug-cc-pVTZ, and UB3LYP/aug-cc-pVTZ levels, respectively.

[g] Obtained by summing up the experimental exoergicity (Ref. 40) (see Table I).

much closer to the value estimated from experimental data.

DFT calculations at the UB3LYP/aug-cc-pVTZ level give very good results [e.g., an energy barrier of 5.81 kcal/mol (6.03 kcal/mol including zero point energy differences)] and compare very well with the highest accurate *ab initio* calculations. Nevertheless, a large spin contamination was observed in TS1 ($\langle S^2\rangle$ was 2.15 to be compared with the correct expectation value of 0.75).

Schaefer III *et al.*,[20] from an early *ab initio* study, proposed the existence of a NOO (A') peroxy isomer as a stable species that could play an important role in atmospheric chemistry. The same authors confirmed later this point by using much more accurate *ab initio* calculations.[21] They found a very shallowly bound isomer, 85.3 kcal/mol over the NO_2 molecule at the CISD+Q/QZ+2P level (Table IV), although no TSs were reported for its dissociation. In a latter paper Walch[22] checked the low stability of this minimum, separated from O(^3P)+NO by an energy barrier of only 0.25 kcal/mol [at the MR–ICCI+Q/CASSCF(9,8) level without the inclusion of ZPE differences]. This energy barrier corresponds approximately to that of TS3 (Table V). Here we have found this peroxy minimum (MIN1) at the CASSCF, CASPT2, and UB3LYP levels as is shown in Table IV. Geometry and frequencies are very similar to those previously obtained by the above-mentioned authors. We have obtained an energy with respect to the NO_2 molecule of 81.01, 86.14, and 84.99 kcal/mol at the CASSCF(17,12), CASPT2(17,12) G2, and UB3LYP with the aug-cc-pVTZ basis set, respectively, also very close to the previous results.[21] The most important CSFs for this minimum are

TABLE V. *Ab initio* and DFT properties of several stationary points located on the $^2A'$ PES.[a]

	Method	Basis set	$R_{e(\mathrm{NO})}$/Å	$R_{e(\mathrm{OO})}$/Å	<NOO/°	ω_i/cm^{-1} [b]			$\Delta E^{\neq}$/kcal mol^{-1} [c]
TS2	CASPT2(17,12) G2	aug-cc-pVTZ	1.1428	1.5653	135.41	1660.03	574.86	619.69i	−21.94
	UB3LYP	aug-cc-pVTZ	1.1324	1.5571	131.83	1748.03	540.27	455.75i	−21.53
TS3	CASPT2(17,12) G2	aug-cc-pVTZ	1.1798	1.4739	114.72	1553.46	390.79	802.04i	−20.00
	UB3LYP	aug-cc-pVTZ	1.1580	1.4942	111.76	1595.70	431.66	751.10i	−21.17
	MR-ICCI+Q/CASSCF(9,8)[d]	cc-pVTZ	1.194	1.483	107.3	1714	602	484i	−14.33
TS4	CASPT2(17,12) G2	aug-cc-pVTZ	1.1415	2.1468	90.15	1891.41	341.35i	139.54	−28.28
	UB3LYP	aug-cc-pVTZ	1.1254	2.2932	89.81	1948.49	276.31i	195.97	−34.89
MIN2	CASPT2(17,12) G2	aug-cc-pVTZ	1.1367	1.9357	117.64	1924.33	344.76	222.14	−30.74
	UB3LYP	aug-cc-pVTZ	1.1255	2.1875	117.59	1961.25	267.55	171.51	−36.56

[a] CASPT2(17,12) G2 energies, geometries, and harmonic vibrational frequencies derived from a grid of points by using the SURVIBTM program (Ref. 33).

[b] Harmonic frequencies: ω_1 (NO str, a'), ω_2 (NOO bend, a'), and ω_3 (OO str, a'), respectively. Masses of the most abundant isotopes were used: ^{14}N and ^{16}O.

[c] Energy barrier respect to N(^4S)+O_2.

[d] Reference 22.

$$\begin{aligned}
&0.917 \quad \cdots(4a')^2(5a')^2(6a')^2(7a')^2(8a')^2(9a')^2(10a')^1(11a')^0(12a')^0(1a'')^2(2a'')^2(3a'')^0,\\
&-0.222 \quad \cdots(4a')^2(5a')^2(6a')^2(7a')^2(8a')^2(9a')^2(10a')^1(11a')^0(12a')^0(1a'')^2(2a'')^0(3a'')^2,\\
&0.108 \quad \cdots(4a')^2(5a')^2(6a')^2(7a')^2(8a')^2(9a')^2(10a')^1(11a')^0(12a')^0(1a'')^2(2a'')^1(3a'')^1,
\end{aligned} \tag{4}$$

where their coefficients are also reported. For this minimum we have also performed calculations using the full valence active space (17,12), and we have seen that increasing the size of the basis set slightly decreases the bond lengths. The geometry optimized at the CASPT2 level is very close to the CASSCF one, with the main difference being observed in the OO distance, which is shorter at the CASPT2 level. As a consequence of this OO shortening the OO stretching frequency is higher at the CASPT2 level compared to the CASSCF one.

From this peroxy minimum two TSs (i.e., TS2 and TS3) with almost no energy barrier over MIN1 lead directly to products $O(^3P)+NO$ (direct mechanism) or to another shallow minimum (MIN2), respectively. In spite of the good fit obtained for the *ab initio* points grids around MIN1 and TS2 (i.e., a root-mean-square deviation below 5×10^{-3} kcal/mol), as their energies at the CASPT2 level are very close (Fig. 1), a somewhat lower energy for TS2 (0.45 kcal/mol) has been achieved, due to the uncertainty in the use of numerical derivatives. Nevertheless, the UB3LYP method, which uses analytical derivatives, gives the correct location.

The minimum MIN2 is a previous step in the indirect insertion mechanism through the NO_2 molecule to produce also $O(^3P)+NO$. TS4 connects MIN2 and the NO_2 molecule. MIN2 and TS4 correspond to C_s stationary points with a lengthened OO bond to allow for the N atom insertion. The absence of energy barriers above reactants apart from the one corresponding to TS1 opens a competition between both kinds of microscopic reaction mechanisms: direct C_s-abstraction and indirect C_s-insertion. The alternative C_{2v}-insertion mechanism, which involves different PESs and their crossings and conical intersections, is under study in our group. The importance of the indirect C_s-insertion mechanism has been observed in a recent wave packet time-dependent quantum dynamics study[51] by using our previous $^2A'$ PES.[10] Although this analytical PES does not properly reproduce the NO_2 geometry [a linear $D_{\infty h}$ minimum is present at -151.3 kcal/mol respect to $O(^3P)+NO$] and fits and estimated energy barrier for the C_{2v} approach [i.e., 47.46 kcal/mol respect to $N(^4S)+O_2$], it presents similar stationary points to the present MIN2 and TS4, which allow the access to the deep linear minimum. This produces a particularly high contribution of the C_s-insertion mechanism and a decrease in the overall reactivity. The importance of the C_s-insertion mechanism has also been observed by us in a preliminary QCT study using a new analytical PES based in the present *ab initio* data.

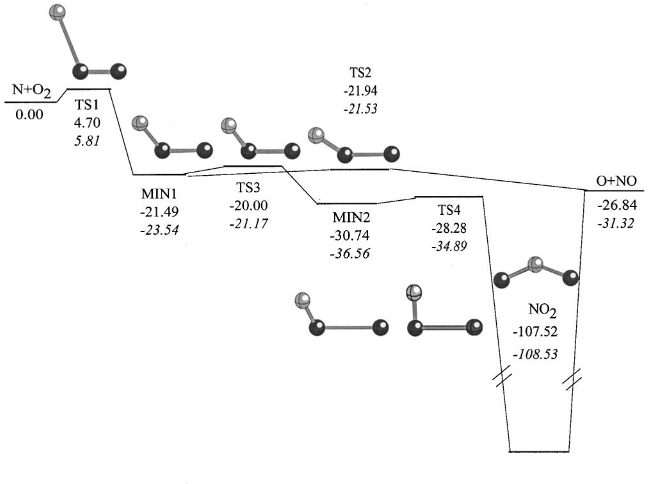

FIG. 1. The lowest $^2A'$ PES MERP at the CASPT2(17,12) G2 (regular numbers) and UB3LYP (italic numbers) levels with the aug-cc-pVTZ basis set. Energies are given relative to reactants, $N(^4S)+O_2$, in kcal/mol.

The NO_2 molecule does not present a potential energy barrier for the ground state dissociation [i.e., $O(^3P)+NO$] in agreement with preceding *ab initio* studies of its photodissociation[52] or unimolecular dissociation.[45]

C. Characterization of the lowest $^4A'$ potential energy surface

The geometries, harmonic vibrational frequencies, and energies relative to reactants, $N(^4S)+O_2$, for all the stationary points characterized at the *ab initio* (i.e., CASSCF and CASPT2) and DFT (i.e., UB3LYP) levels for the lowest quartet PES are shown in Tables VI and VII. Figure 2 depicts the MERP connecting reactants and products, which is much simpler than for the doublet PES. All stationary points display C_s symmetry. The highest energy barrier corresponds to TS1′, whose values are compared in Table VI. CASSCF calculations with different basis sets and the lower active space (11,9) provide resembling geometries, frequencies, and energy barriers.

The increase in the active space to (17,12) produces a significant enlargement of the NO distance (ca., 0.020 Å) and a little energy barrier decrease. The introduction of the dynamical correlation energy through the CASPT2 method (std or G2) originates a large decrease in the energy barrier. The numerical optimization at the CASPT2(17,12) G2 level gives a geometry (Table VI) for TS1′ with a much longer NO distance (i.e., 1.7803 Å) and a shorter OO distance (i.e., 1.2559 Å). An energy barrier of 12.74 kcal/mol (12.79 kcal/mol including ZPE differences) is obtained at the CASPT2(17,12) G2/aug-cc-pVTZ level. The estimated CASPT2(17,12) CBS limits for this energy barrier were (a) 13.06 and 12.82 kcal/mol at the G2 level and (b) 14.38 and 13.80 kcal/mol at the std. level, for cc-pVnZ and aug-cc-pVnZ series, with a maximum error of ± 0.3 kcal/mol, estimated by using other exponential functions. The main difference in both CBS limits (ca. 1.6 kcal/mol) arises again from

TABLE VI. *Ab initio* and DFT properties for the entrance channel transition state (TS1′) on the $^4A'$ PES.[a]

Method	Basis set[b]	E/a.u.	$R_{e(\mathrm{NO})}$/Å	$R_{e(\mathrm{OO})}$/Å	<NOO/°	ω_i/cm^{-1} [c]			$\Delta E^{\neq}$/kcal mol^{-1} [d]
CASSCF(11,9)	ANO-A	−204.118 630	1.6775	1.2740	107.02	637.62*i*	428.23	1153.66	27.95(28.00)
	cc-pVDZ	−204.050 250	1.6554	1.2889	106.04	638.95*i*	434.76	1094.41	29.50(29.49)
	cc-pVTZ	−204.104 769	1.6779	1.2750	106.81	644.14*i*	426.93	1154.05	28.00(28.05)
	cc-pVQZ	−204.119 088	1.6793	1.2712	106.98	643.04*i*	428.40	1165.84	27.89(27.95)
	aug-cc-pVDZ	−204.064 530	1.6737	1.2785	106.21	650.45*i*	413.76	1308.07	27.94(28.18)
	aug-cc-pVTZ	−204.107 672	1.6828	1.2733	107.02	647.97*i*	413.61	1311.54	27.53(27.79)
CASPT2(11,9) std	cc-pVDZ	−204.419 042							21.84
	cc-pVTZ	−204.633 391							17.61
	cc-pVQZ	−204.744 755							16.45
	aug-cc-pVDZ	−204.466 923							18.44
	aug-cc-pVTZ	−204.654 803							15.35
CASPT2(11,9) G2	cc-pVDZ	−204.412 745							19.62
	cc-pVTZ	−204.625 376							15.10
	cc-pVQZ	−204.736 094							13.86
	aug-cc-pVDZ	−204.459 359							16.14
	aug-cc-pVTZ	−204.646 043							12.89
CASSCF(17,12)	ANO-A	−204.127 828	1.6967	1.2724	107.33	637.58*i*	407.92	1166.36	25.56(25.62)
	cc-pVDZ	−204.059 758	1.6747	1.2863	106.37	642.23*i*	414.11	1110.30	26.93(26.92)
	cc-pVTZ	−204.113 893	1.6976	1.2733	107.16	644.71*i*	406.69	1166.18	25.66(25.70)
	cc-pVQZ	−204.128 258	1.6981	1.2696	107.25	642.24*i*	409.18	1178.40	25.52(25.57)
	aug-cc-pVDZ	−204.073 784	1.6947	1.2762	106.43	633.22*i*	391.36	1314.98	25.52(25.75)
	aug-cc-pVTZ	−204.116 817	1.7020	1.2714	107.32	368.28*i*	402.94	1170.50	25.17(25.22)
CASPT2(17,12) std	cc-pVDZ	−204.420 994							21.00
	cc-pVTZ	−204.634 745							16.88
	cc-pVQZ	−204.746 022							15.81
	aug-cc-pVDZ	−204.468 858							17.54
	aug-cc-pVTZ	−204.656 206							14.65
CASPT2(17,12) G2	ANO-A	−204.608 718							12.52
	cc-pVDZ	−204.413 876							19.24
	cc-pVTZ	−204.625 855							14.98
	cc-pVQZ	−204.736 420							13.74
	aug-cc-pVDZ	−204.460 319							15.79
	aug-cc-pVTZ	−204.646 475							12.73
CASPT2(17,12) G2[e]	aug-cc-pVTZ	−204.646 467	1.7803	1.2559	105.65	417.71*i*	355.42	1260.84	12.74(12.79)
UB3LYP	aug-cc-pVTZ		1.9206	1.2218	111.29	406.55*i*	328.96	1428.27	14.18(14.38)
CASSCF(11,9)[f]	Duijneveldt [11s6p/5s3p2d1f]		1.669	1.288	109.9	612*i*	365	1187	27.1(27.1)
MR–CCI+Q/CASSCF(11,9)[f]	Duijneveldt [11s6p/5s3p2d1f]		1.752	1.248	109.4	689*i*	367	1406	18.0(18.3)

[a] CASPT2 energies at the CASSCF optimum geometries with the same basis set.

[b] ANO-A basis set: [14s9p4d3f/4s3p2d1f] (Ref. 36).

[c] Harmonic vibrational frequencies: ω_1 (NO str, a'), ω_2 (NOO bend, a'), and ω_3 (OO str, a'), respectively. Masses of the most abundant isotopes were used: ^{14}N and ^{16}O.

[d] Energy barrier respect to N(^4S)+O_2. The value corrected with the difference of zero point energies is shown in parentheses.

[e] CASPT2 G2 optimum geometries and harmonic vibrational frequencies obtained by using the SURVIBTM program (Ref. 33).

[f] Reference 18.

the use of the G2 or standard CASPT2 variants, as it happens for the TS1 in the doublet PES. The present energy barriers are somewhat lower than the energy barrier fitted in a previous analytical quartet PES[23] (i.e., 15.0 kcal/mol) based on MR–CCI+Q/CASSCF(11,9)/[11s6p/5s3p2d1f] calculations,[18] which presented a original value of 18.0 kcal/mol but with a very similar geometry to the CASPT2(17,12) G2 one (Table VI). We have also calculated the TS1′ energy barrier using the MR–CI+Q/aug-cc-pVTZ method with 11 electrons correlated (N and O 1s and 2s electrons were kept frozen), as for the doublet PES to compare with previous *ab initio* data.[18] An energy barrier of 15.51 kcal/mol was determined by using a MR–CI calculation with 12 CSFs of reference, which is very close to the mentioned published data. CASPT2(11,9) G2 calculations without 2s electron correlation increases the barrier to 16.07 kcal/mol, which is very similar to the aforementioned MR–CI+Q value. Therefore, the 2s electron correlation becomes very important in both the CASPT2 and MR–CI calculations to calculate the energy barrier for both doublet and quartet PESs. The lower energy barrier found for the TS1′ in the quartet PES respect previous published data will produce larger thermal rate constants at high temperatures, where this excited PES becomes quite important [e.g., at 1500 K the $k(^4A')$ contributes around a 10% of the total rate constant].

DFT calculations at the UB3LYP/aug-cc-pVTZ level provide too long NO distances (i.e., 1.9206 Å) although a similar energy barrier of 14.18 kcal/mol (14.38 kcal/mol including ZPE differences). Some spin contamination was also

TABLE VII. *Ab initio* and DFT properties of other stationary points located on the $^4A'$ PES.[a]

	Method	Basis set	$R_{e(\mathrm{NO})}$/Å	$R_{e(\mathrm{OO})}$/Å	<NOO/°	ω_i/cm^{-1} [b]			ΔE/kcal mol^{-1} [c]
TS3′	CASSCF(17,12)	aug-cc-pVTZ	1.3168	1.5023	104.95	1060.75	441.36	740.23*i*	19.59
	CASPT2(17,12) G2	aug-cc-pVTZ	1.2795	1.5183	102.77	1227.53	392.29	775.14*i*	7.81
	UB3LYP	aug-cc-pVTZ	1.2724	1.5266	106.92	1164.60	397.00	780.17*i*	0.93
MIN1′	CASSCF(17,12)	aug-cc-pVTZ	1.3846	1.3861	104.58	999.01	466.76	650.80	18.65
	CASPT2(17,12) G2	aug-cc-pVTZ	1.3779	1.3546	102.73	1058.28	418.36	656.67	5.43
	UB3LYP	aug-cc-pVTZ	1.3769	1.3601	105.30	1058.77	436.30	741.28	−1.58

[a] CASPT2(17,12) G2 energies, geometries, and harmonic vibrational frequencies derived from a grid of points by using the SURVIBTM program (Ref. 33).

[b] Harmonic vibrational frequencies: ω_1 (NO str, a'), ω_2 (NOO bend, a'), and ω_3 (OO str, a'), respectively. Masses of the most abundant isotopes were used: ^{14}N and ^{16}O.

[c] Energy barrier respect to N(^4S)+O$_2$.

observed in TS1′ ($\langle S^2\rangle$ was 4.20 to be compared with the correct expectation value of 3.75).

TS1′ leads to a very shallow minimum (MIN1′) with a structure comparable to the peroxy minimum in the doublet PES. This minimum dissociates to O(^3P)+NO products through TS3′, which has an energy barrier (7.81 kcal/mol) below that of TS1′. Hence, only a direct microscopic mechanism is expected for this PES differing from the double mechanism proposed for the doublet PES. DFT calculations at the UB3LYP/aug-cc-pVTZ level exactly corroborate the *ab initio* MERP.

IV. CONCLUSIONS AND REMARKS

This work presents a detailed theoretical study of the N(^4S)+O$_2$($X\,^3\Sigma_g^-$)→NO($X\,^2\Pi$)+O(^3P) exothermic reaction on its lowest $^2A'$ and $^4A'$ potential energy surfaces. *Ab initio* CASSCF, CASPT2, and MR–CI methods with standard correlation-consistent (cc-pVnZ and aug-cc-pVnZ, n=D, T, Q, 5) Dunning's basis sets and small and large atomic natural orbital basis sets were used; CBS limits were also reported for the main energy barriers (TS1 and TS1′). DFT methods were also used to facilitate the search of the stationary points, producing similar results too. Thus, several minima and transition states have been found along the different MERPs connecting reactants and products on both surfaces.

The ground $^2A'$ PES presents an average energy barrier (TS1) of 4.8 kcal/mol and 5.8 kcal/mol in the CBS limits for the G2 and std CASPT2 levels, respectively. The second value is almost coincident with the energy barrier (6.2 kcal/mol) derived from thermal rate constants in our previous paper. A peroxy NOO minimum is found in agreement with preceding *ab initio* works, which seems to play an important role in the opening of a double microscopic reaction mechanism: direct C_s-abstraction and indirect C_s-insertion. The importance of this second mechanism through the NO$_2$ molecule has been recently anticipated in a wave packet time-dependent quantum dynamics study on our previous analytical doublet PES and also in our preliminary QCT study.

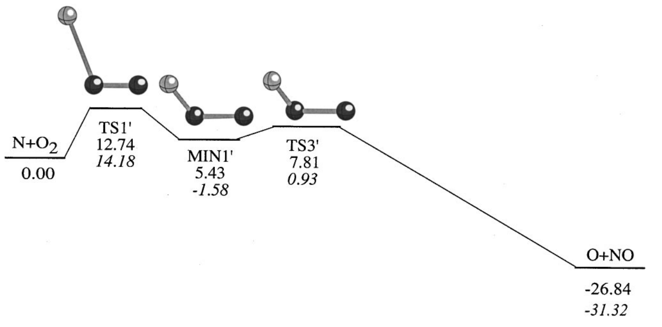

FIG. 2. The lowest $^4A'$ PES MERP at the CASPT2(17, 12) G2 (regular numbers) and UB3LYP (italic numbers) levels with the aug-cc-pVTZ basis set. Energies are given relative to reactants, N(^4S)+O$_2$, in kcal/mol.

The alternative C_{2v}-insertion mechanism with the different PESs and their crossings and conical intersections is currently under study in our group.

The ground $^4A'$ PES presents an average energy barrier (TS1′) of 12.9 kcal/mol and 14.1 kcal/mol in the CBS limits for the G2 and std CASPT2 levels, respectively. In this surface another peroxy minimum is found, although in this case only a direct C_s-abstraction mechanism should be expected.

The present results improve previous high quality *ab initio* studies and provide lower energy barriers for both PESs, which would produce larger values of both thermal rate constants, and therefore a larger total rate constant, with an expected better agreement with the available experimental data.

The good results obtained for reactants and products as well as for the peroxy NOO($^2A'$) minimum and for the NO$_2$($X\,^2A_1$) molecule point towards the suitability of describing both PESs at the CASPT2(17,12) level of theory. Thus, two analytical PESs ($^2A'$ and $^4A'$) based on several grids of *ab initio* points have been almost fitted and dynamics and kinetics studies are currently in progress.

Finally, the study of the N and O 2*s* electron correlation in the MR–CI and CASPT2 methods shows that it is very important to correlate the 2*s* electrons, in both CASPT2 and MR–CI calculations, which produces lower energy barriers, much closer to the value estimated from experimental data. This point was not taken into account in previous *ab initio* studies.

ACKNOWLEDGMENTS

This work has been supported by the "Dirección General de Enseñanza Superior (Programa Sectorial de Promoción General del Conocimiento)" of the Spanish Ministry of Education and Culture (DGES Project ref. PB 98-1209-C02-01). Financial support from the European Union (INTAS Project ref. 99-00701) and the "Generalitat" (Autonomous Government) of Catalonia (Projects refs. 1998SGR 0008 and

2000SGR 00016) is also acknowledged. One of the authors (C.O.) thanks the Spanish Ministry of Education and Culture for a predoctoral research grant. The authors are grateful to the ''Centre de Computació i Comunicacions de Catalunya (C^4-CESCA/CEPBA)'' for providing a part of the computer time. Thanks are also given to Professor Carlo Petrongolo (Università di Siena) for providing us a copy of his recent paper about the time-dependent wave packet study of the $N(^4S)+O_2$ reaction.

[1] M. W. Chase, Jr., C. A. Davies, J. R. Downey, Jr., D. J. Frurip, R. A. McDonald, and A. N. Syverud, J. Phys. Chem. Ref. Data Suppl. **14**, Suppl. 1 (1985).

[2] P. Warneck, in *Chemistry of the Natural Atmosphere* (Academic, San Diego, 1998), Chap. 3.

[3] R. L. Jaffe, M. D. Pattengill, and D. W. Schwenke, in *Supercomputer Algorithms for Reactivity, Dynamics and Kinetics of Small Molecules*, edited by A. Laganà (Kluwer, Dordrecht, 1989), p. 367.

[4] R. D. Sharma, Y. Sun, and A. Dalgarno, Geophys. Res. Lett. **20**, 2043 (1993).

[5] A. Burcat, G. Dixon-Lewis, M. Frenklach, W. C. Gardiner, R. K. Hanson, S. Salimian, J. Troe, J. Warnatz, and R. Zellner, in *Combustion Chemistry*, edited by W. C. Gardiner, Jr. (Springer-Verlag, New York, 1984).

[6] M. Gilibert, A. Aguilar, M. González, and R. Sayós, Chem. Phys. **172**, 99 (1993).

[7] M. Gilibert, A. Aguilar, M. González, and R. Sayós, Chem. Phys. **178**, 178 (1993).

[8] R. Sayós, A. Aguilar, M. Gilibert, and M. González, J. Chem. Soc., Faraday Trans. **89**, 3223 (1993).

[9] M. Gilibert, X. Giménez, M. González, R. Sayós, and A. Aguilar, Chem. Phys. **191**, 1 (1995).

[10] R. Sayós, J. Hijazo, M. Gilibert, and M. González, Chem. Phys. Lett. **284**, 101 (1998).

[11] W. B. DeMore, D. M. Golden, R. F. Hampson, M. J. Kurylo, C. J. Howard, A. R. Ravishankara, C. E. Kolb, and M. J. Molina, in *Chemical Kinetics and Photochemical Data for Use in Stratospheric Modelling*, in Evaluation 12, JPL Publ. 97-4 (Jet Propulsion Lab., Pasadena, CA, 1997).

[12] D. L. Baulch, C. J. Cobos, R. A. Cox, G. Hayman, Th. Just, J. A. Kerr, T. Murrells, M. J. Pilling, J. Troe, R. W. Walker, and J. Warnatz, J. Phys. Chem. Ref. Data **23**, 847 (1994).

[13] M. E. Whitson, Jr., L. A. Darnton, and R. J. McNeal, Chem. Phys. Lett. **41**, 552 (1976).

[14] A. Rahbee and J. J. Gibson, J. Chem. Phys. **74**, 5143 (1981).

[15] R. R. Herm, B. J. Sullivan, and M. E. Whitson, Jr., J. Chem. Phys. **79**, 2221 (1983).

[16] I. C. Winkier, R. A. Stachnik, J. I. Steinfeld, and S. M. Miller, J. Chem. Phys. **85**, 890 (1986).

[17] G. E. Caledonia, R. H. Krech, D. B. Oakes, S. J. Lipson, and W. A. M. Blumberg, J. Geophys. Res. **105**, 12833 (2000).

[18] S. P. Walch and R. L. Jaffe, J. Chem. Phys. **86**, 6946 (1987), and references therein.

[19] G. Suzzi Valli, R. Orrú, E. Clementi, A. Laganà, and S. Crocchianti, J. Chem. Phys. **102**, 2825 (1995).

[20] H. F. Schaefer III, C. F. Bender, and J. H. Richardson, J. Phys. Chem. **80**, 2035 (1976).

[21] C. Meredith, R. D. Davy, G. E. Quelch, and H. F. Shaefer III, J. Chem. Phys. **94**, 1317 (1991).

[22] S. P. Walch, J. Chem. Phys. **102**, 4189 (1995).

[23] J. W. Duff, F. Bien, and D. E. Paulsen, Geophys. Res. Lett. **21**, 2043 (1994).

[24] A. J. C. Varandas and A. I. Voronin, Mol. Phys. **85**, 497 (1995).

[25] D. Bose and G. V. Candler, J. Chem. Phys. **107**, 6136 (1997).

[26] B. Ramachandran, N. Balakrishnan, and A. Dalgarno, Chem. Phys. Lett. **332**, 562 (2000).

[27] N. Balakrishnan and A. Dalgarno, Chem. Phys. Lett. **302**, 485 (1999).

[28] MOLCAS 4.1, K. Andersson, M. R. A. Blomberg, M. P. Fülscher *et al.*, Lund University, Sweden, 1998.

[29] B. O. Roos, P. R. Taylor, and P. E. M. Siegbahn, Chem. Phys. **48**, 157 (1980).

[30] B. O. Roos, in *Advances in Chemical Physics: Ab Initio Methods in Quantum Chemistry-II*, edited by K. P. Lawley (Wiley, New York, 1987), Vol. LXIX, p. 399.

[31] K. Andersson, Theor. Chim. Acta **91**, 31 (1995).

[32] E02 and E04 subroutines from the NAG Fortran Library Mark 15. The Numerical Algorithms Group Ltd., Oxford UK.

[33] W. C. Ermler, H. C. Hsieh, and L. B. Harding, Comput. Phys. Commun. **51**, 257 (1988).

[34] M. González, R. Valero, and R. Sayós, J. Chem. Phys. **113**, 10983 (2000).

[35] T. H. Dunning, Jr., J. Chem. Phys. **90**, 1007 (1989).

[36] P.-O. Widmark, P.-A. Malmqvist, and B. O. Roos, Theor. Chim. Acta **77**, 291 (1990).

[37] Extensible Computational Chemistry Environment Basis Set Database, Version 1.0, as developed and distributed by the Molecular Science Computing Facility, Environmental and Molecular Sciences Laboratory (EMSL) which is a part of the Pacific Northwest Laboratory, P.O. Box 999, Richland, Washington 99352, and funded by the U.S. Department of Energy.

[38] M. J. Frisch, G. W. Trucks, H. B. Schlegel *et al.*, GAUSSIAN 98, Revision A.7, Gaussian, Inc., Pittsburgh, PA, 1998.

[39] M. González, I. Miquel, and R. Sayós, Chem. Phys. Lett. **335**, 339 (2001).

[40] K. P. Huber and G. Herzberg, in *Molecular Spectra and Molecular Structure. Vol. IV. Constants of Diatomic Molecules* (Van Nostrand Reinhold, New York, 1979).

[41] K. A. Peterson, R. A. Kendall, and T. H. Dunning, Jr., J. Chem. Phys. **99**, 9790 (1993).

[42] K. A. Peterson, A. K. Wilson, D. E. Woon, and T. H. Dunning, Jr., Theor. Chem. Acc. **97**, 251 (1997).

[43] G. D. Gillispie, A. U. Khan, A. C. Wahl, R. P. Hosteny, and M. Krauss, J. Chem. Phys. **63**, 3425 (1975).

[44] Y. Xie, R. D. Davy, B. F. Yates, C. P. Blahous III, Y. Yamaguchi, and H. F. Schaefer III, Chem. Phys. **135**, 179 (1989).

[45] S. Yu. Grebenshchikov, C. Beck, H. Flöthman, R. Shinke, and S. Kato, J. Chem. Phys. **111**, 619 (1999).

[46] Landolt-Börnstein, in *Structure Data of Free Polyatomic Molecules*, edited by W. Martienssen (Springer-Verlag, Berlin, 1998), Vol. II/25A.

[47] R. Jost, J. Nygård, A. Pasinski, and A. Delon, J. Chem. Phys. **105**, 1287 (1996).

[48] G. Herzberg, in *Molecular Spectra and Molecular Structure. Vol. III. Electronic Spectra and Electronic Structure of Polyatomic Molecules* (Van Nostrand, New York, 1966).

[49] C. F. Jackels and E. R. Davidson, J. Chem. Phys. **64**, 2908 (1976).

[50] K. A. Peterson and T. H. Dunning, Jr., J. Phys. Chem. A **101**, 6280 (1997).

[51] P. Defazio, C. Petrongolo, S. K. Gray, and C. Oliva, J. Chem. Phys. (to be published).

[52] H. Katagiri and S. Kato, J. Chem. Phys. **99**, 8805 (1993).